Mon. Not. R. Astron. Soc. **000**, 000–000 (2002)

Cosmological constraints from the local X-ray luminosity function of the most X-ray luminous galaxy clusters

S.W. Allen[1], A.C. Fabian[1], R.W. Schmidt[1] and H. Ebeling[2]
1. Institute of Astronomy, Madingley Road, Cambridge CB3 0HA
2. Institute for Astronomy, 2680 Woodlawn Drive, Honolulu, Hawaii 96822, USA

August 22, 2002

ABSTRACT

We present precise constraints on the normalization of the power spectrum of mass fluctuations in the nearby universe, σ_8, as a function of the mean local matter density, $\Omega_{\rm m}$. Using the observed local X-ray luminosity function of galaxy clusters from the extended BCS and REFLEX studies, a mass-luminosity relation determined from Chandra and ROSAT X-ray data and weak gravitational lensing observations, and the mass function predicted by the Hubble Volume simulations of Evrard *et al.* , we obtain $\sigma_8 = (0.469 \pm 0.015)\,\Omega_{\rm m}^{-(0.291\pm0.017)-(0.21\pm0.11)\Omega_{\rm m}}$. The degeneracy between σ_8 and $\Omega_{\rm m}$ can be broken using Chandra measurements of the X-ray gas mass fractions in dynamically relaxed clusters. Using this information, and including Gaussian priors on the mean baryon density of the Universe and the Hubble constant, we obtain $\sigma_8 = 0.710^{+0.025}_{-0.019}$ and $\Omega_{\rm m} = 0.310 \pm 0.008$ for an assumed flat ΛCDM cosmology (marginalized 68 per cent confidence limits). Our results are in good agreement with some recent studies based on the local X-ray temperature function of clusters, the redshift evolution of the X-ray luminosity and temperature functions of clusters, early results from the Sloan Digitized Sky Survey, and the recent analysis of 2dF galaxy redshift survey data and cosmic microwave background anisotropies reported by Lahav *et al.* Our value for σ_8 is $20-35$ per cent lower than current measurements from studies of cosmic shear.

Key words: cosmological parameters – X-rays: galaxies: clusters – gravitational lensing — large-scale structure of the universe — X-rays: galaxies: clusters

1 INTRODUCTION

The X-ray luminosity function of galaxy clusters in the nearby universe provides a powerful cosmological probe. The observed luminosity function, $n(L)$, can be combined with a relation linking the observed X-ray luminosity and mass, and the mass function, $n(M)$, predicted by simulations, to obtain tight constraints on the combination of cosmological parameters $\Omega_{\rm m}$ and σ_8, where $\Omega_{\rm m}$ is the mean matter density of the local universe and σ_8 is the root-mean-square variation of the density field smoothed by a top hat window function of size $8h^{-1}$Mpc.

Observationally, the keys to such studies are precise determinations of the local X-ray luminosity function of clusters and the relation linking the observed X-ray luminosities and total masses. X-ray selection currently offers the best way to identify massive galaxy clusters, and the local X-ray luminosity function has been precisely determined by the BCS (Ebeling *et al.* 1997) and REFLEX (Böhringer *et al.* 2002) studies. These studies, which are based on data from the ROSAT All-Sky Survey (RASS; Trümper 1993), together include $\sim$ 750 clusters and cover approximately two thirds of the sky. Recently, significant effort has also been invested into measuring the local temperature function of clusters (*e.g.* Markevitch 1998; Pierpaoli *et al.* 2001; Ikebe *et al.* 2002), which offers a complementary method for determining cosmological parameters. At present, however, the temperature function samples are significantly smaller than the combined BCS-plus-REFLEX luminosity function data sets.

Recent years have also seen significant efforts directed towards a precise calibration of the 'virial' relations linking the observed luminosities, temperatures and masses of galaxy clusters (*e.g.* Horner, Mushotzky & Scharf 1999; Nevalainen, Markevitch & Forman 2000; Finoguenov, Reiprich & Böhringer 2001; Allen, Schmidt & Fabian 2001b; Sanderson *et al.* 2002). In particular, the launch of the Chandra X-ray Observatory has permitted the first precise measurements of the temperature and mass profiles of relaxed clusters from X-ray data. Using a combination of Chandra and gravitational lensing data, Allen *et al.* (2001b) confirmed that luminous, relaxed galaxy clusters follow the simple scaling relations predicted by theory, but that the normalization of the observed mass-temperature relation mea-

sured within r_{2500} (where the mean enclosed mass density is 2500 times the critical density of the universe at the redshifts of the clusters) is approximately 40 per cent lower than predicted by standard adiabatic simulations. This highlights the likely importance of additional physics such as cooling and pre-heating in the intracluster gas (see also Pearce *et al.* 2000; Thomas *et al.* 2002; Voit *et al.* 2002; Muanwong *et al.* 2002).

Theoretically, the primary requirement for cosmological studies using the observed luminosity and/or temperature functions of clusters is a precise prediction of the mass function. This has now been achieved for flat ΛCDM (and τCDM) cosmologies using the Hubble Volume simulations of Jenkins *et al.* (2001) and Evrard *et al.* (2002).

In this paper we present precise constraints on σ_8 and $\Omega_{\rm m}$ based on the observed local luminosity function of the most X-ray luminous clusters in the extended BCS (Ebeling *et al.* 2000) and REFLEX samples, and a new calibration, using pointed Chandra and ROSAT X-ray observations and weak gravitational lensing results, of the mass-luminosity relation linking the masses of clusters measured within r_{200} to their total $0.1-2.4$ keV ROSAT luminosities. Having determined our combined constraint on σ_8 and $\Omega_{\rm m}$, we show that the degeneracy between these parameters can be broken using Chandra results on the X-ray gas mass fractions in the most dynamically relaxed clusters. Including Gaussian priors on the mean baryon density of the Universe ($\Omega_{\rm b}h^2 = 0.0205 \pm 0.0018$; O'Meara *et al.* 2001) and the Hubble constant ($h = 0.72 \pm 0.08$; Freedman *et al.* 2001), we obtain the final results $\sigma_8 = 0.710^{+0.025}_{-0.019}$ and $\Omega_{\rm m} = 0.310 \pm 0.008$ (marginalized 68 per cent confidence limits for an assumed flat ΛCDM cosmology). We compare our results to other measurements based on the local number density of clusters, evolution of the X-ray luminosity and temperature functions, the 2dF galaxy redshift survey, cosmic microwave background anisotropies, and measurements of cosmic shear.

Throughout this paper, in order to allow direct comparison with the BCS and REFLEX luminosity functions, results on the masses and luminosities of individual clusters are quoted for a flat ΛCDM cosmology with $h = H_0/100\,{\rm km\,s^{-1}\ Mpc^{-1}} = 0.5$, $\Omega_{\rm m} = 0.3$ and $\Omega_\Lambda = 0.7$.

2 THEORY: THE PREDICTED LUMINOSITY FUNCTION OF GALAXY CLUSTERS

Jenkins *et al.* (2001) show that the predicted mass function of galaxy clusters of mass M at redshift z can be written as a function of $\ln\sigma^{-1}(M,z)$, where $\sigma^2(M,z)$ is the variance of the linearly evolved density field smoothed by a spherical top-hat filter of comoving radius R, enclosing a mass $M = 4\pi R^3\bar{\rho}_0/3$. Here $\bar{\rho}_0 = \Omega_{\rm m}(0)\rho_{\rm c}(0)$ is the mean comoving matter density of the universe, $\Omega_{\rm m}(0)$ is the mean, present matter density in units of the critical density, and $\rho_{\rm c}(0) = 3H_0^2/8\pi G$ is the critical density at redshift zero.

Using a spherical overdensity algorithm to measure the masses of clusters within radii r_{200}, where the mean enclosed mass density is 200 times the critical density of the Universe at the redshift of interest, Evrard *et al.* (2002) show that, for a flat ΛCDM ($\Omega_{\rm m} = 0.3, \Omega_\Lambda = 0.7$) cosmology, the mass fraction $f(\sigma^{-1})$ is

$$f(\sigma^{-1}) \ = \ 0.22\exp[-|\ln\sigma^{-1} + 0.73\,|^{3.86}], \qquad (1)$$

and that the differential number density of clusters with mass M at redshift z is

$$\frac{{\rm d}\,n(M,z)}{{\rm d}\ln\sigma^{-1}} = \frac{f(\sigma^{-1})\bar{\rho}(z)}{M}, \qquad (2)$$

where $\bar{\rho}(z) = \bar{\rho}_0(1+z)^3$ is the mean mass density of the universe at redshift z. Following Viana & Liddle (1999), we write

$$\sigma(R,z) = \sigma_8(z)\left(\frac{R}{8h^{-1}\ {\rm Mpc}}\right)^{-\gamma(R)}, \qquad (3)$$

where

$$\gamma(R) = (0.3\Gamma + 0.2)\left[2.92 + \log_{10}\left(\frac{R}{8h^{-1}\ {\rm Mpc}}\right)\right] \qquad (4)$$

and Γ is the shape parameter of the cold dark matter transfer function. Following Sugiyama (1995) we set

$$\Gamma = \Omega_{\rm m}(0){\rm h}\left(\tfrac{2.7{\rm K}}{T_0}\right)^2\exp\left(-\Omega_{\rm b}(0) - \sqrt{\tfrac{h}{0.5}}\tfrac{\Omega_{\rm b}(0)}{\Omega_{\rm m}(0)}\right), \qquad (5)$$

where $T_0 = 2.726$K is the temperature of the cosmic microwave background (Mather *et al.* 1994) and $\Omega_{\rm b}(0) = (0.0205 \pm 0.0018)h^{-2}$ (O'Meara *et al.* 2001) is the mean, present-day baryon density in units of the critical density. The redshift-dependent quantity $\sigma_8(z)$ is related to its present value, $\sigma_8(0)$, by

$$\sigma_8(z) = \sigma_8(0)\,\frac{g(\Omega_{\rm m}(z))}{g(\Omega_{\rm m}(0))}\,\frac{1}{1+z}\,, \qquad (6)$$

where, for a flat ΛCDM universe

$$g(\Omega_{\rm m}(z)) = \frac{5}{2}\Omega_{\rm m}(z)\left[\frac{1}{70} + \frac{209\Omega_{\rm m}(z)}{140} - \frac{\Omega_{\rm m}(z)^2}{140} + \Omega_{\rm m}(z)^{4/7}\right]^{-1} \qquad (7)$$

and

$$\Omega_{\rm m}(z) = \Omega_{\rm m}(0)\,\frac{(1+z)^3}{1-\Omega_{\rm m}(0)+(1+z)^3\Omega_{\rm m}(0)}. \qquad (8)$$

e.g. Viana & Liddle (1996). Combining equations 2 and 3, we obtain

$$\frac{{\rm d}\,n(M,z)}{{\rm d}\,M} = \frac{\gamma\bar{\rho}(z)}{3M^2}f(\sigma^{-1}). \qquad (9)$$

In Section 3.2.4 we show that for clusters with X-ray luminosities, L, exceeding $10^{45}\ {\rm erg\,s^{-1}}$ in the $0.1-2.4$ keV ROSAT band, the mass M measured within r_{200} can be related to the luminosity by a power-law model of the form

$$E(z)M = M_0\left[\frac{L}{E(z)}\right]^\alpha, \qquad (10)$$

where the best fit values and uncertainties on M_0 and α are determined from Chandra and ROSAT X-ray data and weak gravitational lensing results and

$$E(z) = (1+z)\sqrt{(1+z\Omega_{\rm m}+\Omega_\Lambda/(1+z)^2-\Omega_\Lambda)} \qquad (11)$$

(*e.g.* Bryan & Norman 1998). Applying the chain rule we obtain

$$\frac{{\rm d}\,n(L,z)}{{\rm d}\,L} = \frac{\gamma\bar{\rho}(z)\alpha}{3M_0}\left[\frac{E(z)}{L}\right]^{\alpha+1} f(\sigma^{-1}). \qquad (12)$$

The predicted differential luminosity function (*i.e.* the comoving number density of clusters at redshift z with luminosities in an interval ${\rm d}L$ around L) given by equation 12 can be compared with the observed X-ray luminosity function from the BCS and REFLEX studies to constrain the combination of cosmological parameters $\Omega_{\rm m}(0)$ and $\sigma_8(0)$, hereafter referred to as $\Omega_{\rm m}$ and σ_8, respectively.

3 OBSERVATIONS

3.1 The observed X-ray luminosity function of the most luminous galaxy clusters in the RASS

For this study, we concentrate on the local ($z \lesssim 0.3$) X-ray luminosity function and restrict ourselves to the most luminous clusters, with $L_{\rm X} > 10^{45}\,{\rm erg\,s^{-1}}$ in the $0.1-2.4$ keV ROSAT band (for a cosmology with $h=0.5$, $\Omega_{\rm m}=0.3$ and $\Omega_\Lambda = 0.7$). This selection is facilitated by the large sample size and well-determined selection functions of the BCS and REFLEX data sets.

The restriction to high luminosities reduces systematic uncertainties by matching the luminosity range of the luminosity function data to the range over which the mass-luminosity relation has been calibrated (Section 3.2.4). At lower luminosities, the effects of pre-heating and cooling in the intracluster gas are expected to become important and cause the mass-luminosity and mass-temperature relations to deviate from simple power-law forms (*e.g.* Cavaliere, Menci & Tozzi 1997). Since the most massive clusters provide the most powerful constraints on cosmological parameters, relatively little information is lost by restricting ourselves to the largest systems.

The binned X-ray luminosity functions for clusters with $L_{\rm X,0.1-2.4} > 10^{45}\,{\rm erg\,s^{-1}}$ from the northern extended BCS (Ebeling *et al.* 2000) and southern REFLEX (Böhringer *et al.* 2002) studies are summarized in Table 1. The mean redshift of the BCS clusters in this luminosity range is $z = 0.21$.*

* We make the comparison between the observed and predicted luminosity functions at $z = 0.21$, the mean redshift of the BCS clusters with $L_{\rm X,0.1-2.4} > 10^{45}\,{\rm erg\,s^{-1}}$. Shifting this redshift by ± 0.05 does not significantly change the results.

Table 1. The observed, binned X-ray luminosity function of the highest luminosity ($L_{\rm X,0.1-2.4} > 10^{45}\,{\rm erg\,s^{-1}}$) galaxy clusters from the extended BCS and REFLEX studies. Column 2 gives the mean $0.1-2.4$ keV X-ray luminosity for each bin. Error bars indicate the bin boundaries. Column 3 gives the number of clusters in each bin and column 4 the comoving space density in ${\rm Mpc^{-3}}$ $(10^{44}\,{\rm erg\,s^{-1}})^{-1}$. A ΛCDM cosmology with $h=0.5$, $\Omega_{\rm m}=0.3$ and $\Omega_\Lambda=0.7$ is assumed.

	$L_{\rm X}$	$n_{\rm clus}$	$n(L)$
BCS	$11.73^{+1.62}_{-1.73}$	17	$1.32 \pm 0.32 \times 10^{-9}$
	$15.65^{+2.20}_{-2.30}$	17	$7.45 \pm 1.81 \times 10^{-10}$
	$23.91^{+28.8}_{-6.06}$	17	$8.10 \pm 1.97 \times 10^{-11}$
REFLEX	$11.25^{+2.19}_{-1.19}$	20	$1.56 \pm 0.34 \times 10^{-9}$
	$16.27^{+4.61}_{-2.83}$	20	$4.44 \pm 0.98 \times 10^{-10}$
	$29.95^{+76.2}_{-9.07}$	20	$1.77 \pm 0.39 \times 10^{-11}$

Table 2. Summary of the Chandra observations. The dates of the observations are given in column 3. Column 4 lists the exposure times in ks.

	z	Date	Exposure
PKS0745-191	0.103	2001 Jun 16	17.9
Abell 963	0.206	2000 Oct 11	36.3
Abell 2390	0.230	1999 Nov 07	9.1
Abell 2667	0.233	2001 Jun 19	9.6
Abell 1835	0.252	1999 Dec 12	19.6
Abell 611	0.288	2001 Nov 03	36.1
MS2137-2353	0.313	1999 Nov 18	20.6
RXJ1347-1145	0.451	2000 Mar 05/Apr 29	18.9
3C295	0.461	1999 Aug 30	17.0

3.2 The observed mass-luminosity relation for luminous galaxy clusters

In determining the mass-luminosity relation we have used mass measurements obtained from Chandra X-ray observations of dynamically relaxed clusters and weak gravitational lensing results drawn from the literature. X-ray luminosities are determined from pointed ROSAT observations. In total, the sample used to define the mass-luminosity relation includes 16 clusters with precise mass estimates and X-ray luminosities $L_{X,0.1-2.4} > 10^{45}\,{\rm erg\,s^{-1}}$, spanning the redshift range $0.1 < z < 0.46$.

3.2.1 Chandra mass measurements

The Advanced CCD Imaging Spectrometer (ACIS) on Chandra permits direct, simultaneous measurements of the X-ray gas temperature and density profiles and, via the hydrostatic assumption, the total mass distributions in galaxy clusters. We have used Chandra to obtain precise mass measurements for a sample of nine of the most X-ray luminous, dynamically relaxed clusters identified from the RASS. The relaxed dynamical states of the clusters are demonstrated by their regular X-ray and optical morphologies, X-ray temper-

Table 3. Summary of the Chandra mass measurements. Column 2 gives the evolution parameter, $E(z)$, appropriate for each cluster. Columns 3 and 4 summarize the best-fitting NFW model parameters: the scale radius, r_s (in Mpc) and concentration parameter, c. Columns 5 and 6 give the virial radii, r_{200} (in Mpc) and masses, M_{200} (in $10^{14}\,\mathrm{M}_\odot$). Error bars are 68 per cent confidence limits for a single interesting parameter. A ΛCDM cosmology with $\Omega_\mathrm{m}=0.3, \Omega_\Lambda=0.7$ and $h=0.5$ is assumed.

	$E(z)$	r_s	c	r_{200}	M_{200}
PKS0745-191	1.050	$0.90^{+0.13}_{-0.17}$	$3.83^{+0.52}_{-0.27}$	$3.44^{+0.20}_{-0.27}$	$26.0^{+4.9}_{-5.6}$
Abell 963	1.107	$0.42^{+0.14}_{-0.07}$	$5.72^{+0.78}_{-1.07}$	$2.40^{+0.20}_{-0.15}$	$9.86^{+2.74}_{-1.77}$
Abell 2390	1.122	$1.06^{+2.23}_{-0.55}$	$3.20^{+1.79}_{-1.57}$	$3.40^{+1.95}_{-0.82}$	$28.9^{+83.6}_{-16.2}$
Abell 2667	1.124	$0.98^{+0.67}_{-0.29}$	$3.02^{+0.74}_{-0.85}$	$2.96^{+0.63}_{-0.38}$	$19.0^{+14.9}_{-6.4}$
Abell 1835	1.135	$0.77^{+0.25}_{-0.13}$	$4.21^{+0.53}_{-0.61}$	$3.24^{+0.44}_{-0.19}$	$25.5^{+11.7}_{-4.2}$
Abell 611	1.158	$0.56^{+0.97}_{-0.25}$	$4.58^{+2.36}_{-2.22}$	$2.56^{+1.04}_{-0.43}$	$13.1^{+23.3}_{-5.5}$
MS2137-2353	1.174	$0.22^{+0.04}_{-0.04}$	$8.71^{+1.22}_{-0.92}$	$1.95^{+0.12}_{-0.14}$	$5.95^{+1.17}_{-1.23}$
RXJ1347-1145	1.271	$0.52^{+0.25}_{-0.17}$	$6.34^{+1.61}_{-1.35}$	$3.28^{+0.56}_{-0.50}$	$33.2^{+19.9}_{-13.0}$
3C295	1.279	$0.22^{+0.10}_{-0.06}$	$7.90^{+1.71}_{-1.72}$	$1.77^{+0.22}_{-0.18}$	$5.27^{+2.23}_{-1.43}$

ature maps and, in 6/9 cases, from the availability of consistent, independent mass measurements from gravitational lensing studies (see Section 4.3).

The Chandra observations were made using the ACIS and the back-illuminated S3 detector between 1999 August 30 and 2001 November 3. We have used the level-2 event lists provided by the standard Chandra pipeline processing. These lists were cleaned for periods of background flaring using the CIAO software package, resulting in the net exposure times summarized in Table 2.

The data have been analysed using the methods described by Allen *et al.* (2001a, 2002b) and Schmidt *et al.* (2001; these papers present detailed mass analyses of Abell 2390, RXJ1347-1145 and Abell 1835, respectively). In brief, concentric annular spectra were extracted from the cleaned event lists, centred on the peaks of the X-ray emission from the clusters. (For RXJ1347-1145, the data from the south-east quadrant of the cluster were excluded due to ongoing merger activity in that region; Allen *et al.* 2002b.) The spectra were analysed using XSPEC (version 11.0: Arnaud 1996), the MEKAL plasma emission code (Kaastra & Mewe 1993; incorporating the Fe-L calculations of Liedhal, Osterheld & Goldstein 1995), and the photoelectric absorption models of Balucinska-Church & McCammon (1992; the absorbing column density was included as a free parameter in the fits, thereby alleviating problems associated with uncertainties in the quantum efficiency of the detectors at low energies). Only data in the $0.5-7.0$ keV energy range were used. The spectra for all annuli were modelled simultaneously in order to determine the deprojected X-ray gas temperature profiles, under the assumption of spherical symmetry.

For the mass modelling, azimuthally averaged surface brightness profiles were constructed from background subtracted, flat-fielded images with a 0.984×0.984 arcsec^2 pixel scale (2×2 raw detector pixels). When combined with the deprojected spectral temperature profiles, the surface brightness profiles can be used to determine the X-ray gas mass and total mass profiles in the clusters.† For this analysis, we have used an enhanced version of the image deprojection code described by White, Jones & Forman (1997) with distances calculated using the code of Kayser, Helbig & Schramm (1997).

We have parameterized the cluster mass (luminous plus

† The observed surface brightness profile and a particular parameterized mass model are together used to predict the temperature profile of the X-ray gas. (We use the median temperature profile determined from 100 Monte-Carlo simulations. The outermost pressure is fixed using an iterative technique which ensures a smooth pressure gradient in these regions.) The predicted temperature profile is rebinned to the same binning as the spectral results and the χ^2 difference between the observed and predicted, deprojected temperature profiles is calculated. The parameters for the mass model are stepped through a regular grid of values in the r_s-c or r_s-σ planes to determine the best-fitting values and 68 per cent confidence limits. (The best-fit models generally provide good descriptions of the data). The gas mass profile is determined to high precision at each grid point directly from the observed surface brightness profile and model temperature profile. Spherical symmetry and hydrostatic equilibrium are assumed throughout.

Table 4. Summary of the mass results from the Dahle *et al.* (2002) weak lensing observations. Columns 2 and 3 summarize the redshifts and evolution parameters for the clusters. Column 4 lists the virial masses, M_{200} (in $10^{14}\,\mathrm{M}_\odot$), determined from fits to the observed tangential shear profiles using NFW models with a fixed concentration parameter, $c=5$. Error bars are 68 per cent confidence limits for a single interesting parameter. A ΛCDM cosmology with $\Omega_\mathrm{m}=0.3, \Omega_\Lambda=0.7$ and $h=0.5$ is assumed.

	z	$E(z)$	M_{200}
Abell 520	0.203	1.106	$12.8^{+4.5}_{-3.9}$
Abell 209	0.206	1.107	$4.0^{+2.1}_{-1.8}$
Abell 141	0.230	1.122	$11.9^{+6.8}_{-5.5}$
Abell 267	0.230	1.122	$13.6^{+3.9}_{-3.5}$
Abell 1576	0.299	1.165	$15.0^{+3.6}_{-3.3}$
Abell 1995	0.320	1.179	$16.6^{+3.9}_{-3.5}$
Abell 1351	0.328	1.184	$35.6^{+6.4}_{-6.0}$

dark matter) profiles using a Navarro, Frenk & White (1997; hereafter NFW) model with

$$\rho(r) = \frac{\rho_{\rm c}(z)\delta_{\rm c}}{(r/r_{\rm s})\,(1+r/r_{\rm s})^2}, \qquad (13)$$

where $\rho(r)$ is the mass density, $\rho_{\rm c}(z) = 3H(z)^2/8\pi G$ is the critical density for closure at redshift z, $r_{\rm s}$ is the scale radius, c is the concentration parameter ($c = r_{200}/r_{\rm s}$) and $\delta_{\rm c} = 200c^3/3\,[\ln(1+c) - c/(1+c)]$. The normalizations of the mass profiles can also be expressed in terms of an effective velocity dispersion, $\sigma = \sqrt{50}\,r_{\rm s}cH(z)$ (with $r_{\rm s}$ in units of Mpc and $H(z)$ in $\rm km\,s^{-1}\ Mpc^{-1}$).

The best-fit NFW parameter values and 68 per cent confidence limits are summarized in Table 3. This table also lists the 'virial' radii, r_{200}, where the mean enclosed density is 200 times the critical density of the universe at the redshifts of the clusters, and the masses within these radii, M_{200}. Note that the Chandra data only cover the central regions of the clusters out to radii $0.3 - 0.5\,r_{200}$ and thus some extrapolation of the models, assuming that the NFW parameterization remains valid to r_{200}, is required in calculating the virial masses.

3.2.2 Weak lensing mass measurements

In order to expand the sample of clusters used to construct the mass-luminosity relation, we have also included data for clusters for which accurate mass measurements are available from weak gravitational lensing studies. Since lensing mass measurements are essentially independent of the dynamical state of the gravitating matter, the inclusion of such clusters also allows us to ensure that our results are not biased by a restriction to dynamically relaxed systems. This is important because the BCS and REFLEX luminosity functions are X-ray flux-limited samples and contain clusters with a range of dynamical states.

The weak lensing results used here are primarily drawn from the study of Dahle *et al.* (2002). Their results include aperture mass profiles for eight clusters with $L_{X,0.1-2.4} > 10^{45}\,\rm erg\,s^{-1}$ (Section 3.2.3) obtained from wide-field imaging with the University of Hawaii (UH) 2.24m telescope and UH8K camera. One of these clusters, Abell 963, is also included in our Chandra sample. Since the Chandra and lensing data give consistent results on M_{200} and the Chandra data provide tighter constraints, we do not use the lensing data for Abell 963 here. The weak lensing mass measurements made with the UH8K camera use a control annulus of 550 arcsec, corresponding to $1.7h^{-1}$Mpc for a cluster at $z = 0.3$.

We have used the aperture mass profiles presented by Dahle *et al.* (2002) to recover the mean tangential shear profiles for the clusters and have fitted these with NFW models. In general, the lensing data are unable to constrain both the concentration parameter and scale radius of the NFW models and so we have fixed $c = 5$ for this analysis, a typical value for such massive clusters inferred from simulations (*e.g.* Navarro *et al.* 1997), and consistent with the Chandra results listed in Table 3. The masses of the clusters determined from the Dahle *et al.* (2002) data are summarized in Table 4.

In addition to the Dahle *et al.* (2002) UH8K data, accurate weak lensing mass measurements are also available for Abell 2390 (Squires *et al.* 1996) and RXJ1347-1145 (Fischer & Tyson 1997). In both cases the lensing mass measurements at r_{200} are in good agreement with the Chandra results (Allen *et al.* 2001a, 2002b). Dahle *et al.* (2002) also present a weak lensing mass measurement for Abell 1835 using a smaller camera, which is consistent with the Chandra result in Table 3.

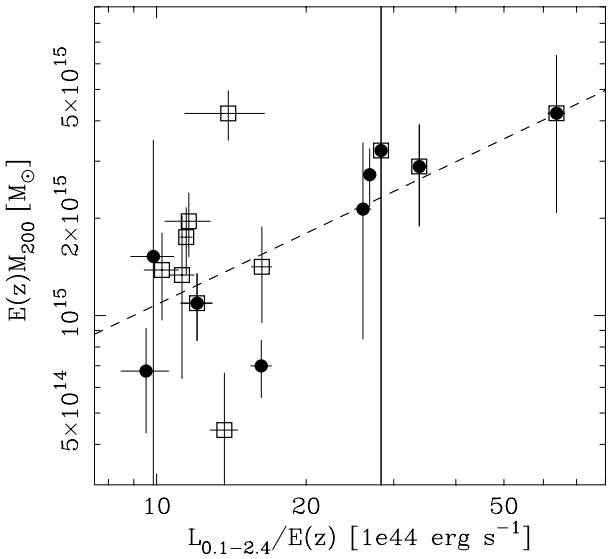

Figure 1. The observed mass-luminosity relation. Chandra mass measurements are indicated by filled circles. Weak lensing mass measurements are indicated by open squares. The four clusters with Chandra mass measurements and consistent weak lensing results are indicated by filled circles surrounded by open squares. The data for Abell 267 have been offset slightly for display purposes. The best-fitting power law model from Section 3.2.4 is shown as the dashed curve. The two most significant outliers above (Abell 1351) and below (Abell 209) the best-fit curve appear to be undergoing major merger events (see Section 4.3). A ΛCDM cosmology with $\Omega_{\rm m} = 0.3, \Omega_\Lambda = 0.7$ and $h = 0.5$ is assumed.

3.2.3 ROSAT luminosity measurements

In constructing the mass-luminosity relation, we have used pointed ROSAT observations to determine the total, intrinsic $0.1 - 2.4$ keV luminosities of the clusters to high precision. This minimizes systematic uncertainties by matching the observing band and (as far as possible) detector technology to that used for the RASS observations. The agreement between the BCS and REFLEX fluxes, which are based on RASS data, and the fluxes determined from deep, pointed ROSAT observations is good (Ebeling *et al.* 1998; Böhringer *et al.* 2002). The details of the pointed ROSAT observations are summarized in Table 5. The data were analysed using the XSELECT package (version 2.0) and XSPEC (version 11.0). The emission-weighted temperatures and metallicities of the clusters were set to the values measured with Chandra. Where Chandra data were not available, the metallicity was set to 0.3 solar and the temperature was determined iteratively from the luminosity-temperature relation of Allen

Table 5. Summary of the pointed ROSAT observations. Columns 3 and 4 list the date of observation and the detector used. Column 5 gives the exposure times in ks. Column 6 lists the intrinsic $0.1-2.4$ luminosities, $L_{0.1-2.4}$ (in $10^{44}\,\mathrm{erg\,s^{-1}}$). Error bars are 68 per cent confidence limits. A ΛCDM cosmology with $\Omega_\mathrm{m}=0.3, \Omega_\Lambda=0.7$ and $h=0.5$ is assumed.

	z	Date	Detector	Exposure	$L_{0.1-2.4}$
PKS0745-191	0.103	1993 Oct 15	PSPC	10.5	28.2 ± 0.6
Abell 520	0.203	1998 Mar 09	HRI	27.7	18.0 ± 0.8
Abell 209	0.206	1996 Jul 01	HRI	10.6	15.2 ± 1.0
Abell 963	0.206	1991 Apr 20	HRI	10.5	13.4 ± 1.0
Abell 141	0.230	1996 Dec 10	HRI	16.2	12.6 ± 0.7
Abell 267	0.230	1996 Jan 03	HRI	15.7	11.1 ± 0.9
Abell 2390	0.230	1993 Nov 13	PSPC	10.3	31.7 ± 0.5
Abell 2667	0.233	1994 Dec 14	HRI	21.3	29.2 ± 1.1
Abell 1835	0.252	1993 Jul 03	PSPC	6.2	38.3 ± 0.9
Abell 611	0.288	1996 Apr 04	HRI	17.3	11.4 ± 1.1
Abell 1576	0.299	1993 Nov 07	PSPC	16.3	13.4 ± 0.4
MS2137-2353	0.313	1993 Nov 07	PSPC	10.5	19.1 ± 0.9
Abell 1995	0.320	1995 Nov 13	HRI	16.5	13.7 ± 1.4
Abell 1351	0.328	1995 Apr 29	HRI	31.9	16.5 ± 3.0
RXJ1347-1145	0.451	1995 Jan 28	HRI	15.8	81.1 ± 3.1
3C295	0.461	1995 Jun 19	HRI	22.2	12.2 ± 1.3

& Fabian (1998). Note, however, that the precise settings of the temperatures and metallicities have little effect on the measured $0.1-2.4$ keV luminosities for such hot, massive clusters. The absorbing column densities were set to the Galactic values determined by Dickey & Lockman (1990).

The intrinsic $0.1-2.4$ keV luminosities for a ΛCDM cosmology with $\Omega_\mathrm{m}=0.3, \Omega_\Lambda=0.7$ and $h=0.5$ (the same cosmology assumed in the BCS and REFLEX luminosity functions in Table 1) are listed in Table 5.

3.2.4 The observed mass-luminosity relation

The mass-luminosity relation for the 16 X-ray luminous clusters in our sample, measured within radii r_{200} corresponding to a density contrast $\Delta=200$ with respect to the critical density of the universe at the redshifts of the clusters, is shown in Fig. 1. Those clusters with mass measurements from Chandra X-ray data are indicated by filled circles. Clusters with weak lensing mass measurements are marked with open squares. The four clusters with Chandra mass measurements and consistent weak lensing results are indicated by filled circles surrounded by open squares. A ΛCDM cosmology with $\Omega_\mathrm{m}=0.3, \Omega_\Lambda=0.7$ and $h=0.5$ is assumed.

We have fitted the data using a simple power-law model of the form

$$E(z)\left[\frac{M_{200}}{1\ \mathrm{M}_\odot}\right] = M_0\left[\frac{L}{E(z)\,10^{44}\,\mathrm{erg\,s^{-1}}}\right]^\alpha. \quad (14)$$

Using the BCES($X_2|X_1$) estimator of Akritas & Bershady (1996), which accounts for errors in both axes and the presence of possible intrinsic scatter, we obtain best-fitting values and 68 per cent confidence limits from 1000 bootstrap simulations of $M_0 = 2.16^{+1.27}_{-0.87}\times10^{14}\,\mathrm{M}_\odot$ and $\alpha = 0.73^{+0.15}_{-0.14}$. Repeating the analysis using only the nine clusters with Chandra mass measurements, we find $M_0 = 1.03^{+0.92}_{-0.53}\times$

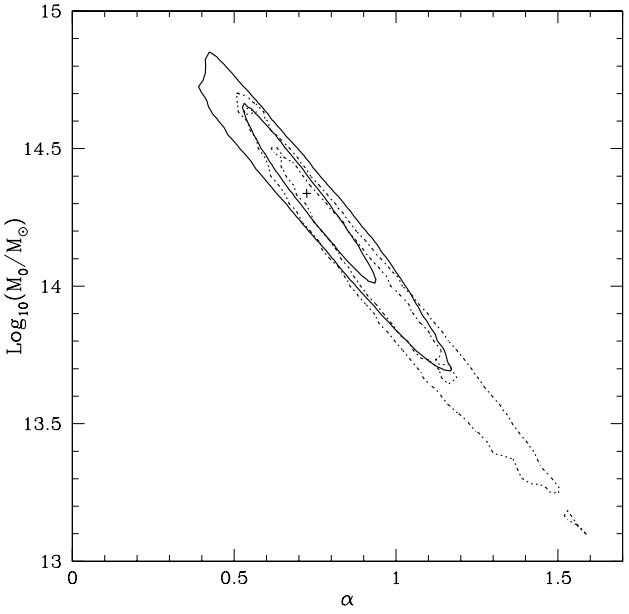

Figure 2. The 68.3 and 95.4 per cent confidence contours on the normalization, M_0, and slope, α, of the power-law model fitted to the mass-luminosity data. The solid curves show the results obtained for all 16 clusters using both the Chandra and Dahle *et al.* (2002) data. The plus sign marks the best-fit position. The dotted curves show the results obtained using only the nine clusters observed with Chandra.

$10^{14}\,M_\odot$ and $\alpha = 0.93^{+0.22}_{-0.17}$. The expected slope of the mass–*bolometric* luminosity relation in models of simple gravitational collapse is $\alpha = 0.75$. The distribution of M_0 and α values are shown in Fig. 2.

4 RESULTS

4.1 Constraints on σ_8 as a function of Ω_m

Using the theoretical prescription for the mass function of galaxy clusters described in Section 2, the observed BCS+REFLEX X-ray luminosity function data from Table 1, and the mass-luminosity relation discussed in Section 3.2.4, we can determine σ_8 as a function of Ω_m.

For this analysis we assume a flat ΛCDM cosmology ($\Omega_m + \Omega_\Lambda = 1$). We have examined a grid of parameter values covering the range $0.2 < \sigma_8 < 1.4$ and $0.1 < \Omega_m < 1.0$. For each parameter pair, we use equation 12 and 1000 bootstrap simulations of the mass-luminosity data in Fig. 1 to predict the luminosity function and 68 per cent confidence limits. The χ^2 difference between the observed and predicted luminosity functions is then calculated.

Fig. 3 shows the 1 and 2 sigma confidence contours ($\Delta\chi^2 = 2.30$ and 6.17 corresponding to the 68.3 and 95.4 per cent confidence limits, respectively) in the $\sigma_8 - \Omega_m$ plane. The best-fit curve can be approximated by a simple fitting formula $\sigma_8 = (0.469 \pm 0.015)\,\Omega_m^{-(0.291\pm0.017)-(0.21\pm0.11)\Omega_m}$.

Fig. 4 shows the extended BCS and REFLEX luminosity function data for $L_{X,0.1-2.4} > 10^{45}\,\mathrm{erg\,s^{-1}}$, together with the predicted luminosity function and 68 per cent uncertainties for a cosmology with $\Omega_m = 0.31$ and $\sigma_8 = 0.71$. We see that the predicted curve provides a good description of the observations. The uncertainties in the predicted model, which arise primarily from the uncertainties in the mass-luminosity relation, dominate over the uncertainties in the luminosity function data.

4.2 Breaking the $\sigma_8 - \Omega_m$ degeneracy using the Chandra $f_{gas}(z)$ data

The usual approach, discussed in the literature, to break the degeneracy between σ_8 and Ω_m in Fig. 3 is to use the redshift evolution of the luminosity and/or temperature function of clusters, which depends strongly on the mean mass density of the universe (see references in Section 5.2). However, this approach is both observationally challenging in terms of identifying complete, high-redshift cluster samples, and prone to systematic uncertainties due to increased levels of dynamical activity and contaminating AGN emission at high redshifts, which introduce additional scatter into the mass-luminosity and mass-temperature relations.

Fortunately, the Chandra data offer a powerful alternative method to break the degeneracy between σ_8 and Ω_m, using the observed X-ray gas mass fractions in the clusters, f_{gas}, and their apparent redshift dependence (*e.g.* White & Frenk 1991; White *et al.* 1993; Sasaki 1996; Pen 1997; Ettori & Fabian 1999; Allen *et al.* 2002a; Erdogdu, Ettori & Lahav 2002). The matter content of rich clusters of galaxies is thought to provide a fair sample of the Universe (*e.g.* White *et al.* 1993). The observed ratio of baryonic to total mass in clusters is therefore expected to closely match the ratio of

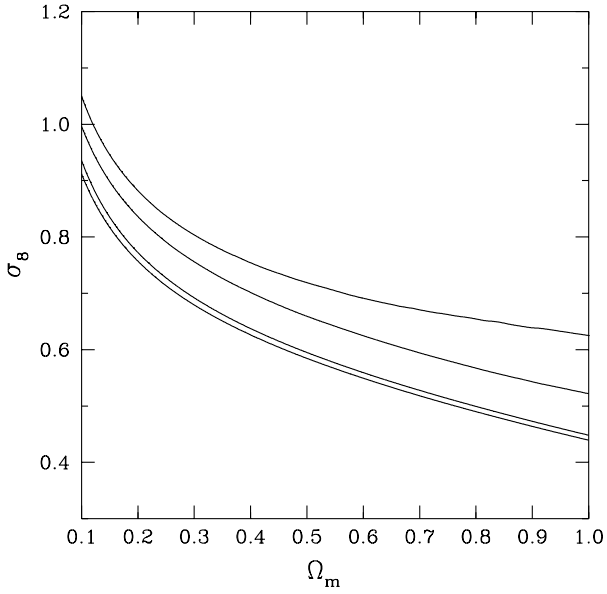

Figure 3. The 68.3 and 95.4 per cent confidence contours ($\Delta\chi^2 = 2.30$ and 6.17, respectively) on σ_8 and Ω_m obtained from the BCS+REFLEX luminosity function data (Table 1) and observed mass-luminosity relation (Section 3.2.4). A flat ΛCDM cosmology is assumed.

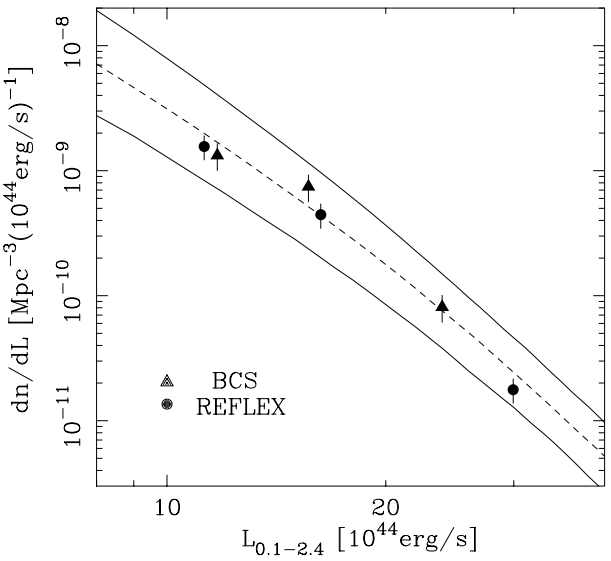

Figure 4. The BCS (triangles) and REFLEX (circles) luminosity functions for clusters with $L_{X.0.1-2.4} > 10^{45}\,\mathrm{erg\,s^{-1}}$, together with the predicted, model luminosity function for a cosmology with $\Omega_m = 0.31$ and $\sigma_8 = 0.71$ (dashed curve) and 68 per cent confidence limits (solid curves) determined from 1000 bootstrap simulations of the mass-luminosity relation. A mean redshift of $z = 0.21$ is assumed.

the cosmological parameters $\Omega_{\rm b}/\Omega_{\rm m}$, where $\Omega_{\rm b}$ is the mean baryon density of the Universe. The apparent redshift dependence of the $f_{\rm gas}$ measurements arises from the fact that the measured $f_{\rm gas}$ values depend upon the assumed angular diameter distances to the sources as $f_{\rm gas} \propto D_{\rm A}^{1.5}$. Thus, although we expect the measured $f_{\rm gas}$ values to be invariant with redshift, this will only appear to be the case when the assumed cosmology matches the true, underlying cosmology.

The observed $f_{\rm gas}$ profiles for the nine relaxed clusters studied with Chandra, for an $h = 0.5$ standard cold dark matter (SCDM) cosmology with $\Omega_{\rm m} = 1.0$ and $\Omega_\Lambda = 0.0$, are shown in Fig. 5. (The six clusters previously studied by Allen *et al.* 2002a are shown in a lighter shading.) With the possible exception of Abell 963, we see that the $f_{\rm gas}$ profiles appear to have converged (or be close to converging) within r_{2500}. Fig. 6 shows the $f_{\rm gas}$ measurements at r_{2500} as a function of redshift, for the eight clusters with convergent $f_{\rm gas}$ profiles. Following Allen *et al.* (2002a), we have fitted these data with the model

$$f_{\rm gas}^{\rm mod}(z) = \frac{\Omega_{\rm b}}{\left(1+0.19\sqrt{h}\right)\Omega_{\rm m}} \left[\frac{h}{0.5}\,\frac{D_{\rm A}^{\Omega_{\rm m}=1,\Omega_\Lambda=0}(z)}{D_{\rm A}^{\Omega_{\rm m},\,\Omega_\Lambda=1-\Omega_{\rm m}}(z)}\right]^{1.5} \quad (15)$$

and determined the best-fitting value of $\Omega_{\rm m}$, for an assumed flat ΛCDM cosmology. We include Gaussian priors on the Hubble constant, $h = 0.72 \pm 0.08$, the final result from the Hubble Key Project reported by Freedman *et al.* (2001), and $\Omega_{\rm b}h^2 = 0.0205 \pm 0.0018$ (O'Meara *et al.* 2001), from cosmic nucleosynthesis calculations constrained by the observed abundances of light elements at high redshifts. The constraints on $\Omega_{\rm m}$ determined from this analysis are shown in Fig. 7. We measure $\Omega_{\rm m} = 0.310^{+0.020}_{-0.018}$ at 68 per cent confidence.

We can now combine the constraints on $\Omega_{\rm m}$ from Fig. 7 with the joint constraints on σ_8 and $\Omega_{\rm m}$ in Fig. 3 to obtain our final results on σ_8 and $\Omega_{\rm m}$, shown in Fig. 8. We measure $\sigma_8 = 0.710^{+0.025}_{-0.019}$ and $\Omega_{\rm m} = 0.310 \pm 0.008$ (marginalized 68 per cent confidence limits).

4.3 Systematic uncertainties and the effects of merger events

An important aspect of the present work is the reduced level of systematic uncertainty with respect to some previous studies based on the local abundance of galaxy clusters. In the first case, the independent BCS and REFLEX studies have well determined selection functions (Ebeling *et al.* 1998, 2000; Böhringer *et al.* 2002) and provide precise, consistent results on the local luminosity function. With the large size of the combined BCS-plus-REFLEX data set (which covers two thirds of the sky) we have been able to limit our analysis to the most luminous clusters, with $L_{X,0.1-2.4} > 10^{45}\,{\rm erg\,s^{-1}}$ (for an $\Omega_{\rm m} = 0.3$, $\Omega_\Lambda = 0.7$, $h = 0.5$ cosmology), for which the mass-luminosity relation has been calibrated using Chandra and ROSAT X-ray data and weak lensing observations (Section 3.2.4). The complicating effects of cooling and pre-heating are minimized for such massive clusters and a simple power-law model provides a reasonable description of the mass-luminosity relation (Fig. 1), albeit with some residual intrinsic scatter that is presumably related to the different dynamical his-

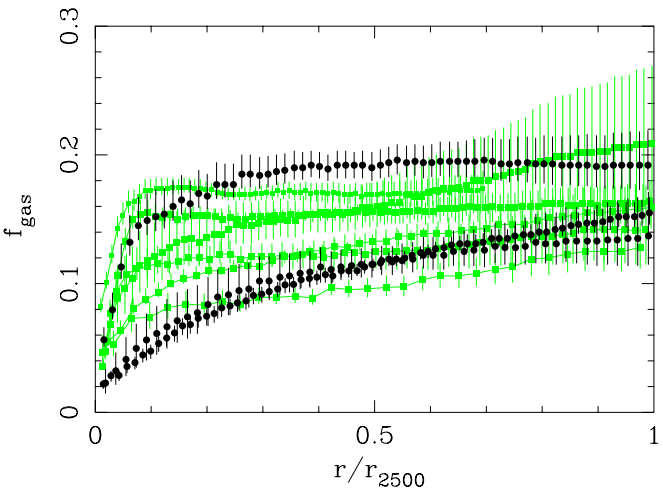

Figure 5. The X-ray gas mass fraction profiles measured with Chandra, with the radial axis scaled in units of r_{2500}. The results for the six clusters previously discussed by Allen *et al.* (2002a) are shown in lighter shading. The new results for Abell 611, 963 and 2667 are shown as dark circles. Note that $f_{\rm gas}(r)$ is an integrated quantity and so the error bars on neighbouring points in a profile are correlated. An SCDM cosmology with $h = 0.5$ is assumed.

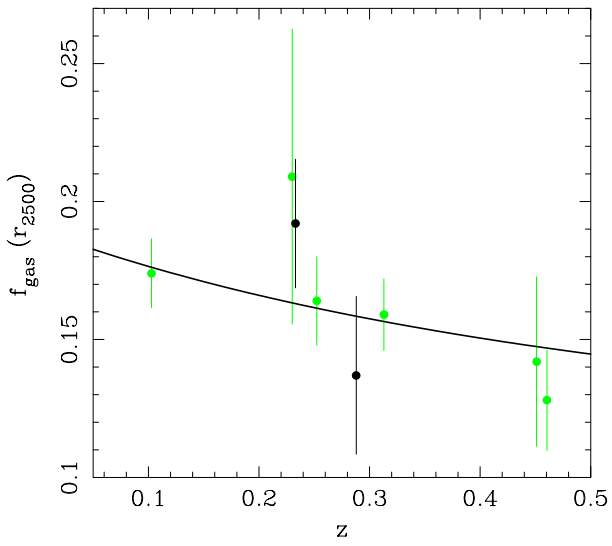

Figure 6. The apparent redshift variation of the X-ray gas mass fraction measured at r_{2500} (with root-mean-square 1σ errors) for the eight clusters with convergent $f_{\rm gas}$ profiles in Fig. 5 (see text). The results for the six clusters previously discussed by Allen *et al.* (2002a) are shown in lighter shading. The solid curve shows the predicted $f_{\rm gas}(z)$ behaviour for a flat ΛCDM cosmology with $\Omega_{\rm m} = 0.31$ and $\Omega_\Lambda = 0.71$.

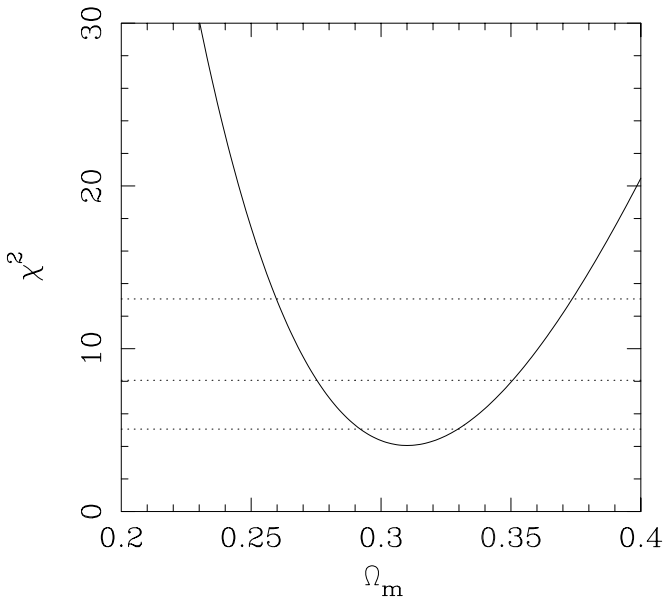

Figure 7. The marginalized constraints on Ω_m from the Chandra $f_{gas}(z)$ data shown in Fig. 6. A flat ΛCDM cosmology and Gaussian priors of $h = 0.72 \pm 0.08$ and $\Omega_b h^2 = 0.0205 \pm 0.0018$ are assumed. The 1, 2 and 3 sigma confidence limits are marked as dotted lines.

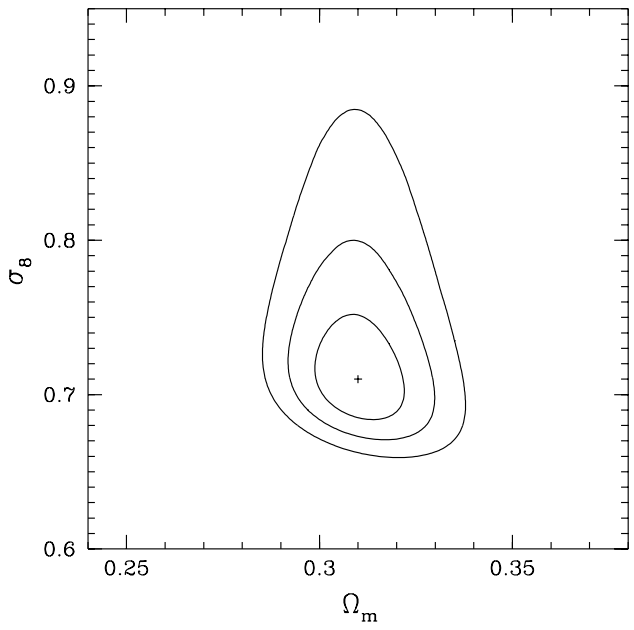

Figure 8. The 1, 2 and 3 sigma confidence contours on σ_8 and Ω_m from the combined analysis of the BCS+REFLEX luminosity function and Chandra $f_{gas}(z)$ data. A flat ΛCDM cosmology is assumed.

tories of the clusters (see below). Repeating the analysis using only the BCS luminosity function data, or only the REFLEX data, or using a higher luminosity cut in the luminosity function (*e.g.* $L_{X,0.1-2.4} > 1.3{\times}10^{45}\,\mathrm{erg\,s^{-1}}$), leads to consistent results (although with larger statistical uncertainties). We note the importance of using an appropriate ΛCDM cosmology in the determinations of the X-ray luminosity function and mass-luminosity relation.

The dominant statistical and systematic uncertainties in the analysis are associated with the mass-luminosity relation. However, care has been taken to minimize the systematic uncertainties. In particular, we have limited our study of the mass-luminosity relation to clusters with precise mass measurements from Chandra and wide-field gravitational lensing studies. The clusters studied with Chandra have been selected from the RASS as the most luminous, dynamically relaxed (in terms of their X-ray and optical morphologies) clusters known. The relaxed natures of these systems means that they are the clusters for which X-ray mass measurements are most reliable. For Abell 963, 1835, 2390 and RXJ1347-1145, independent confirmation of the Chandra mass measurements at r_{200} is available from weak gravitational lensing studies (Dahle *et al.* 2002; Squires *et al.* 1996; Fischer & Tyson 1997; Allen *et al.* 2001a, 2002b). A programme of weak lensing measurements for the other clusters in our Chandra sample is underway (Gray *et al.* , in preparation). In addition, consistent strong lensing mass measurements are available for Abell 1835, 2390, RXJ1347.5-1145, MS2137.3-2353 and PKS0745-191 (Schmidt *et al.* 2001, Allen *et al.* 2001a, 2002b, Schmidt *et al.* , in preparation). The presence of significant non-thermal pressure support on large spatial scales in these clusters can therefore be excluded.

As well as increasing the sample size used in determining the mass-luminosity relation, the inclusion of the Dahle *et al.* (2002) lensing data is important in that it ensures that the analysis is not limited to dynamically relaxed systems. The Dahle *et al.* sample includes clusters with a wide range of dynamical states. Inspection of ROSAT and Chandra images for these clusters shows that they all exhibit significant dynamical activity, with Abell 141, 209, 520, 1351 and 1576 undergoing major merger events. (Similar conclusions are drawn by Dahle *et al.* 2002 from their optical data). The BCS and REFLEX samples, from which the X-ray luminosity functions have been constructed (Section 3.1), include all clusters above the appropriate X-ray flux limits, independent of their dynamical states. It is therefore important that the mass-luminosity relation provides a fair translation between luminosity and mass for all clusters in the BCS and REFLEX samples. From inspection of Fig. 1, it appears that the Dahle *et al.* (2002) clusters have a similar mean mass per unit X-ray luminosity to the relaxed systems studied with Chandra, albeit with two significant outliers from the best-fit curve.

Ricker & Sarazin (2001), Ritchie & Thomas (2002) and Randall, Sarazin & Ricker (2002) present simulations of the effects of mergers on the X-ray properties of clusters for a variety of mass ratios, impact parameters and central gas densities. These authors suggest that major mergers can lead to significant short-term increases in the luminosities of clusters during the periods of closest approach, which are then followed by dips in luminosity as the merging dark

matter cores move apart, before the cluster returns to equilibrium. From Fig. 1 we see that Abell 209 appears to have an unusually high X-ray luminosity/mass ratio, which may have been boosted by the ongoing merger activity in this cluster. (We note, however, that MS2137.3-2353, which is a highly relaxed cluster with no obvious merger activity and a sharp central density peak, also appears to have a high luminosity/mass ratio and lies below the best-fitting curve. In this case the offset may indicate a relatively early formation epoch for the cluster.) In contrast Abell 1351, which is also undergoing a major merger event, has an unusually low X-ray luminosity/mass ratio and lies above the best-fit curve in Fig. 1. Detailed simulations and further observations are required to improve our understanding of the effects of mergers on the X-ray properties of clusters. However, the indications from the present study are that the effects of mergers on the mass-luminosity relation for the most luminous clusters are relatively small. Excluding the Dahle *et al.* (2002) data and limiting our analysis of the mass-luminosity relation to only the dynamically relaxed clusters observed with Chandra leads to consistent results on σ_8 and $\Omega_{\rm m}$.

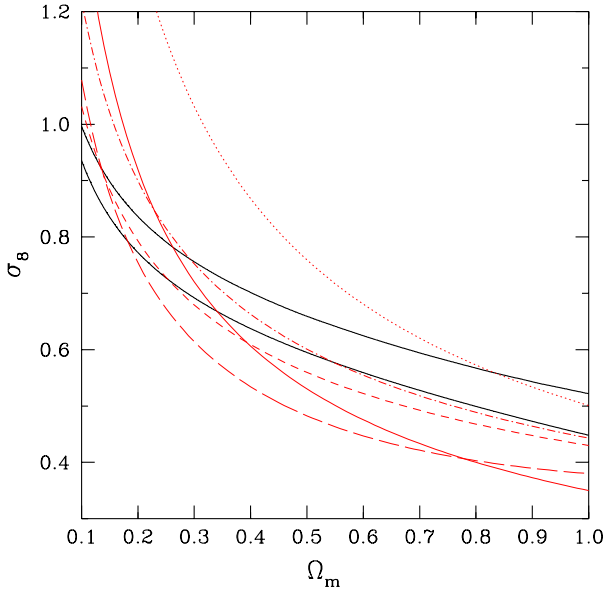

Figure 9. The 68 per cent confidence contours on σ_8 as a function of $\Omega_{\rm m}$ determined from the present study (thick, solid curves; as in Fig. 3) together with the best-fit results of Seljak (2002: dot-dashed curve), Pierpaoli *et al.* (2001: dotted curve), Reiprich & Böhringer (2001: short-dashed curve), Viana *et al.* (2002: long-dashed curve) and Bahcall *et al.* (2002: thin, solid curve). See text for details. A flat ΛCDM cosmology is assumed.

5 COMPARISON WITH OTHER RESULTS

5.1 Other local cluster abundance studies

Fig. 9 shows a comparison of the results on σ_8 as a function of $\Omega_{\rm m}$ from the present study (thick, solid curves: as in Fig. 3), with the findings from five other recent studies based on the observed local number density of galaxy clusters. The dot-dashed curve in Fig. 9 shows the result of Seljak (2002), $\sigma_8 = (0.44 \pm 0.04)\,\Omega_{\rm m}^{-0.44}(\Gamma/0.2)^{0.08}$, using the observed local X-ray temperature function of rich clusters (Pierpaoli, Scott & White 2002) and a mass-temperature relation determined from ASCA and ROSAT observations (Finoguenov *et al.* 2001). The result of Seljak is in good agreement with ours for $\Omega_{\rm m} \sim 0.3$, although the present study leads to tighter constraints. The result of Pierpaoli *et al.* (2001), $\sigma_8 = (0.50 \pm 0.04)\,\Omega_{\rm m}^{-0.60}$ (dotted curve), based on the same local temperature function data but normalized by a theoretical mass-temperature relation, lies significantly above ours. The result of Reiprich & Böhringer (2001), $\sigma_8 = 0.43\,\Omega_{\rm m}^{-0.38}$ (short dashes), based on ASCA and ROSAT observations of RASS selected clusters, is in good agreement with the present study for $\Omega_{\rm m} \lesssim 0.3$. The result of Viana, Nichol & Liddle (2002), $\sigma_8 = 0.38\,\Omega_{\rm m}^{-0.48+0.27\,\Omega_{\rm m}}$ (long dashes), using the local REFLEX X-ray luminosity function and a mass-luminosity relation determined from ROSAT X-ray observations and a stacked weak lensing analysis of relatively low-mass clusters identified in Sloan Digitized Sky Survey (SDSS) commissioning data, lies below our result for $\Omega_{\rm m} \geq 0.2$. Finally, the result of Bahcall *et al.* (2002), $\sigma_8 = 0.35\,\Omega_{\rm m}^{-0.60}$, obtained by combining the number density of optically-selected, relatively low-mass clusters observed in SDSS commissioning data with a mass-optical richness correlation, is in good agreement with this work for $\Omega_{\rm m} \sim 0.3$.

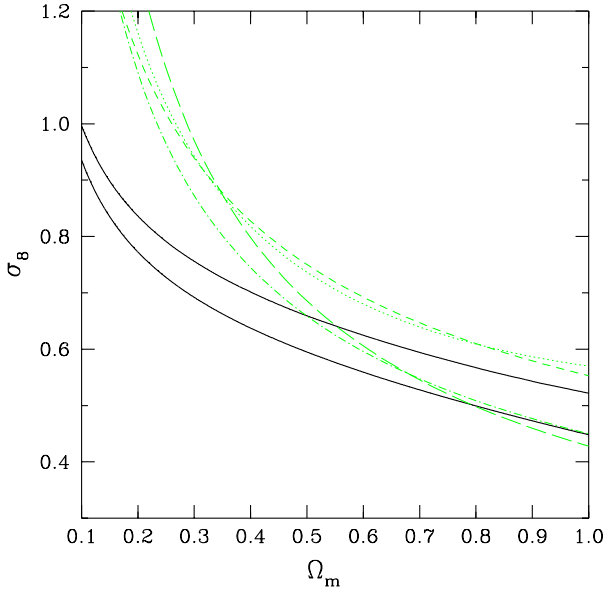

Figure 10. The 68 per cent confidence contours on σ_8 as a function of $\Omega_{\rm m}$ from the present study (dark, solid curves; as in Fig. 3) together with the best-fit results from the cosmic shear studies of Van Waerbeke *et al.* (2002: dotted curve), Refregier *et al.* (2002: short-dashed curve), Bacon *et al.* (2002: long-dashed curve) and Hoekstra *et al.* (2002: dot-dashed curve). A flat ΛCDM cosmology is assumed.

5.2 Evolution in the X-ray luminosity and temperature functions

Borgani *et al.* (2001) present constraints on σ_8 and $\Omega_{\rm m}$ determined from an analysis of evolution in the X-ray luminosity function of clusters in the ROSAT Deep Cluster Survey, which spans the redshift range $z \lesssim 1.3$. Their results of $\sigma_8 = 0.66^{+0.06}_{-0.05}$ and $\Omega_{\rm m} = 0.35^{+0.13}_{-0.10}$ for a flat ΛCDM cosmology are consistent with those reported here.

Donahue & Voit (1999) report results from an analysis of evolution in the temperature function of clusters within $z \lesssim 0.8$, using the low-redshift cluster sample of Markevitch (1998) and a high redshift sample identified from the Einstein Observatory Extended Medium Sensitivity Survey (EMSS). Their results, for an assumed flat ΛCDM cosmology, of $\sigma_8 = 0.73^{+0.03}_{-0.05}$ and $\Omega_{\rm m} = 0.27 \pm 0.10$ are in good agreement with ours. Eke *et al.* (1998) obtain $\sigma_8 = 0.75 \pm 0.15$ and $\Omega_{\rm m} = 0.36 \pm 0.25$ (flat ΛCDM) from an analysis of the temperature function within $z \sim 0.4$, which is consistent with the present work. Our results are marginally inconsistent with the values of $\sigma_8 = 0.72 \pm 0.10$ and $\Omega_{\rm m} = 0.49 \pm 0.12$ reported by Henry (2000) from an independent analysis combining the local temperature function of clusters with the properties of EMSS clusters within $z < 0.6$.

5.3 Cosmic shear measurements

Fig. 10 shows a comparison of the results on σ_8 as a function of $\Omega_{\rm m}$ determined from the present study (dark, solid curves: as in Fig. 3) together with the findings from four recent studies based on measurements of weak gravitational lensing due to large scale structure (cosmic shear). The dotted curve in Fig. 10 shows the result of Van Waerbeke *et al.* (2002), $\sigma_8 = (0.57 \pm 0.04)\,\Omega_{\rm m}^{(0.24\pm0.18)\Omega_{\rm m}-0.49}$. The short-dashed curve shows the result of Refregier, Rhodes & Groth (2002), $\sigma_8 = (0.55 \pm 0.08)\,\Omega_{\rm m}^{-0.44}$. The long-dashed curve shows the result of Bacon *et al.* (2002), $\sigma_8 = (0.43 \pm 0.06)\,\Omega_{\rm m}^{-0.68}$. Finally, the dot-dashed curve shows the result of Hoekstra, Yee & Gladders (2002), $\sigma_8 = (0.45 \pm 0.05)\,\Omega_{\rm m}^{-0.55}$. The results on σ_8 from the four cosmic shear studies lie $20-35$ per cent above the results from this work for $\Omega_{\rm m} \sim 0.3$. (A flat ΛCDM cosmology is assumed in all cases.) We note that in order to obtain agreement with the cosmic shear results, the mean mass per unit luminosity in this study would need to be raised by a factor ~ 2.5.

5.4 Cosmic microwave background anisotropies and the 2dF galaxy redshift survey

Fig. 11 shows the combined (68 and 95 per cent confidence) constraints on σ_8 and $\Omega_{\rm m}$ obtained from the present study (inner, shaded contours), including the Chandra $f_{\rm gas}(z)$ data and Gaussian priors on the Hubble constant ($h = 0.72 \pm 0.08$) and $\Omega_{\rm b}$ ($\Omega_{\rm b}h^2 = 0.0205 \pm 0.0018$), together with the results from the recent analysis of cosmic microwave background (CMB) anisotropies and 2dF galaxy redshift survey data by Lahav *et al.* (2002). The CMB data consist of a combination of COBE, Boomerang (Netterfield *et al.* 2002; de Bernardis *et al.* 2002), Maxima (Lee *et al.* 2001; Stomper *et al.* 2001) and DASI (Halverson *et al.* 2002; Pryke *et al.* 2002)

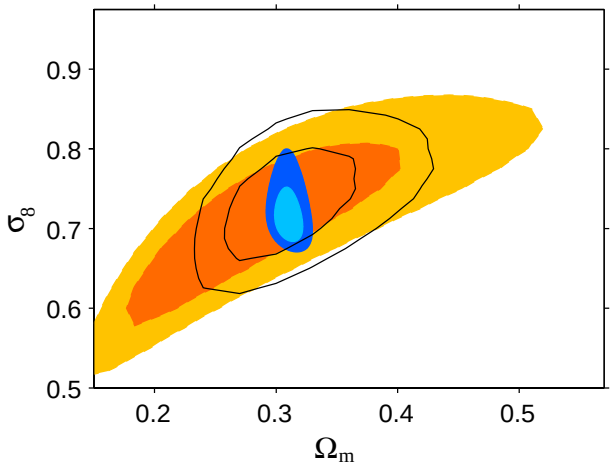

Figure 11. The joint 1 and 2 sigma confidence contours on σ_8 and $\Omega_{\rm m}$ from Lahav *et al.* (2002; outer, filled contours) from their analysis of CMB data, including a Gaussian prior $h = 0.70 \pm 0.07$ and assuming $\Omega_{\rm b}h^2 = 0.020$ (fixed). The open, bold contours show the results of Lahav *et al.* (2002) from their analysis of the combined CMB+2dF data set, marginalizing over h and $\Omega_{\rm b}$. The inner, filled contours show the results from the present study (as in Fig. 8) assuming Gaussian priors of $h = 0.72 \pm 0.08$ and $\Omega_{\rm b}h^2 = 0.0205 \pm 0.0018$. A flat ΛCDM cosmology is assumed in all cases.

data. The results obtained from the CMB data alone, using a Gaussian prior $h = 0.70 \pm 0.07$ and fixing $\Omega_{\rm b}h^2 = 0.020$, the spectral index $n = 1$, and the optical depth due to reionization $\tau = 0$, are shown as the outer, filled contours. The results obtained from the combined CMB+2dF data set, marginalizing over h and $\Omega_{\rm b}$, are shown as solid lines. A flat ΛCDM cosmology is assumed throughout. We see that the results from all three data sets are consistent at the 68 per cent confidence level. Our results are also in good agreement with the recent re-analysis of the CMB+2dF data reported by Percival *et al.* (2002), the studies of CMB data by Lewis & Bridle (2002) and Melchiorri & Silk (2002), and results from CMB data and Type Ia supernovae presented by Jaffe *et al.* (2001).

6 IMPLICATIONS FOR OTHER WORK

The constraints on cosmological parameters reported here ($\sigma_8 = 0.710^{+0.025}_{-0.019}$ and $\Omega_{\rm m} = 0.310 \pm 0.008$ for an assumed flat ΛCDM cosmology) are consistent with, though tighter than, those obtained from a number of other, recent studies based on the local X-ray temperature function of galaxy clusters, and evolution in the X-ray temperature and luminosity functions. Our results are also in good agreement with recent findings from studies of anisotropies in the CMB, the distribution of galaxies in the 2dF galaxy redshift survey, the properties of type Ia supernovae, and early results on large scale structure from the SDSS. Our measurement of σ_8 is, however, $20-35$ per cent lower than the most recent values inferred from studies of cosmic shear. The origin of the dis-

crepancy with the cosmic shear results remains unclear at present.

Our results have a number of implications for other cosmological studies. Firstly, the agreement between the cluster, CMB and 2dF results in Fig. 11 requires that the optical depth to reionization is not large ($\tau \lesssim 0.1$; this issue will be examined in more detail in future work). Secondly, our result on σ_8 implies that the possible excess power detected at high multipoles ($l \sim 2000 - 3000$) in the CMB anisotropy power spectrum with the Cosmic Background Imager (Mason *et al.* 2002; Bond *et al.* 2002) is probably not due to the Sunyaev-Zeldovich (SZ) effect. Our results also have important implications for future X-ray and SZ clusters surveys, since the number of clusters detected at high redshifts with high X-ray luminosities, temperatures and SZ fluxes will be much lower in a $\sigma_8 \sim 0.7$ universe than predicted by simulations with $\sigma_8 \sim 1$.

Finally, we suggest that given the precision of the constraints on $\Omega_{\rm m}$ available from current Chandra $f_{\rm gas}(z)$ data for relaxed clusters, and the relatively small systematic uncertainties involved (see also the discussion in Allen *et al.* 2002a), the $f_{\rm gas}(z)$ data should be considered as a powerful probe for future cosmological work, complementary to measurements of redshift evolution in the X-ray temperature and luminosity functions of galaxy clusters.

Acknowledgements

We are grateful to George Efstathiou for a number of helpful discussions and suggestions. We thank Sarah Bridle and Andrew Liddle for comments, and Ofer Lahav and Sarah Bridle for providing the CMB and 2DF results shown in Fig. 11. We thank Alastair Edge and Carolin Crawford their efforts in the compilation of the extended BCS sample. SWA and ACF acknowledge the support of the Royal Society. HE acknowledges financial support from NASA grant NAG 5-8253 and CXO grant GO1-2132X.

REFERENCES

Akritas M.G., Bershady M.A., 1996, ApJ, 470, 706
Allen S.W., Fabian A.C., 1998, MNRAS, 297, L57
Allen S.W., Ettori S., Fabian A.C., 2001a, MNRAS, 324, 877
Allen S.W., Schmidt R.W., Fabian A.C., 2001b, MNRAS, 328, L37
Allen S.W., Schmidt R.W., Fabian A.C., 2002a, MNRAS, 334, L11
Allen S.W., Schmidt R.W., Fabian A.C., 2002b, MNRAS, in press (astro-ph/0111368)
Arnaud, K.A., 1996, in Astronomical Data Analysis Software and Systems V, eds. Jacoby G. and Barnes J., ASP Conf. Series volume 101, p17
Bacon D., Massey R., Refregier A., Ellis R., 2002, MNRAS, submitted (0203134)
Bahcall N.A. *et al.* , 2002, ApJ, submitted (astro-ph/0205490)
Balucinska-Church M., McCammon D., 1992, ApJ, 400, 699
Bennett C. *et al.* , 1996, ApJ, 464, L1
Böhringer H. *et al.* 2001, A&A, 368, 86
Böhringer H. *et al.* 2002, ApJ, 566, 93
Bond J.R. *et al.* , 2002, ApJ, submitted (astro-ph/0205386)
Borgani S. *et al.* , 2001, ApJ, 561, 13
Bryan G.L., Norman M.L., 1998, ApJ, 495, 80
Cavaliere A., Menci N., Tozzi P., 1997, ApJ, 484, L21
Dahle H., Kaiser N., Irgens R.J., Lilje P.B., Maddox S., 2002, ApJS, 139, 313
de Bernardis P. *et al.* , 2002, ApJ, 564, 559
Dickey J.M., Lockman F.J., 1990, ARA&A, 28, 215
Donahue M., Voit G.M., 1999, ApJ, 523, L137
Ebeling H., Edge A.C., Henry J.P., 2001, ApJ, 553, 668
Ebeling H., Edge A.C., Fabian A.C., Allen S.W., Crawford C.S., Böhringer H., 1997, ApJ, L101.
Ebeling H., Edge A.C., Böhringer H., Allen S.W., Crawford C.S., Fabian A.C., Voges W., Huchra J.P., 1998, MNRAS, 301, 881
Ebeling H., Edge A.C., Allen S.W., Crawford C.S., Fabian A.C., Huchra J.P., 2000, MNRAS, 318, 333
Eke V.R., Cole S., Frenk C.S., Henry J.P., 1998, MNRAS, 298, 1145
Erdogdu P., Ettori S., Lahav O., 2002, MNRAS, submitted (astro-ph/0202357)
Ettori S., Fabian A.C., 1999, MNRAS, 305, 834
Evrard A.E. *et al.* , 2002, ApJ, in press (astro-ph/0110246)
Finoguenov A., Reiprich T.H., Böhringer H., 2001, A&A, 368, 749
Fischer P., Tyson J.A., 1997, AJ, 114, 14
Freedman W. *et al.* , 2001, ApJ, 553, 47
Fukugita M., Hogan C.J., Peebles P.J.E., 1998, ApJ, 503, 518
Halverson N.W. *et al.* , 2002, ApJ, 568, 38
Henry J.P., 2000, ApJ, 534, 565
Hoekstra H., Yee H.K.C., Gladders M.D., 2002, ApJ, submitted (astro-ph/0204295)
Horner D.J., Mushotzky R.F., Scharf C.A., 1999, ApJ, 520, 78
Ikebe Y., Reiprich T.H., Böhringer H., Tanaka Y., Kitayama T., 2002, A&A, 383, 773
Jaffe A.H. *et al.* , 2001, Phys. Rev. Lett., 86, 3475
Jenkins A., Frenk C.S., White S.D.M., Colberg J.M., Cole S., Evrard A.E., Couchman H.M.P., Yoshida N., 2001, MNRAS, 321, 372
Kaastra J.S., Mewe R., 1993, Legacy, 3, HEASARC, NASA
Kayser R., Helbig P., Schramm T., 1997, A&A, 318, 680
Lahav O. *et al.* , 2002, MNRAS, in press (astro-ph/0112162)
Lee A.T. *et al.* , 2001, ApJ, 561, L1
Lewis A., Bridle S., 2002, preprint (astro-ph/0205436)
Liedhal D.A., Osterheld A.L., Goldstein W.H., 1995, ApJ, 438, L115
Markevitch M., 1998, ApJ, 504, 27
Mason B.S. *et al.* , 2002, ApJ, submitted (astro-ph/0205384)
Mather J.C. *et al.* , 1994, ApJ, 420, 439
Melchiorri A., Silk, J., 2002, Phys. Rev. D, 66, 041301R (astro-ph/0203200)
Muanwong O., Thomas P.A., Kay S., Pearce F.R., 2002, MNRAS, submitted (astro-ph/0205137)
Navarro J.F., Frenk C.S., White S.D.M., 1997,ApJ, 490, 493
Netterfield C.B. *et al.* , 2002, ApJ, in press (astro-ph/0104460)
Nevalainen J., Markevitch M., Forman W., 2000, ApJ, 536, 73
O'Meara J.M., Tytler D., Kirkman D., Suzuki N., Prochaska J.X., Lubin D., Wolfe A.M., 2001, ApJ, 552, 718
Pearce F.R., Thomas, P.A., Couchman H.M.P., Edge A.C., 2000, MNRAS, 317, 1029
Pen U., 1997, NewA, 2, 309
Percival W.J. *et al.* , 2002, MNRAS, submitted (astro-ph/0206256)
Pierpaoli E., Scott D., White M., 2001, MNRAS, 325, 77
Pryke C., Halverson N.W., Leitch E.M., Kovac J., Carlstrom J.E., Holzapfel W.L., Bragovan M., 2002, ApJ, 568, 46
Randall S.W., Sarazin C.L., Ricker P.M., 2002, ApJ, in press (astro-ph/0206161)
Refregier A., Rhodes J., Groth E.J., 2002, ApJL, submitted (astro-ph/0203131)
Reiprich T.H., Böhringer H., 2002, ApJ, 567, 716

Ricker P.M., Sarazin C.L., 2001, ApJ, 561, 621
Ritchie B.W., Thomas P.A., 2002, MNRAS, 329, 675
Sanderson A.J.R., Ponman T.J., Finoguenov A., Lloyd-Davies E.J., Markevitch M., 2002, MNRAS, submitted
Sasaki S., 1996, PASJ, 48, L119
Schmidt R.W., Allen S.W., Fabian A.C., 2001, MNRAS, 327, 1057
Seljak U., 2002, MNRAS, in press (astro-ph/0111362)
Squires G., Kaiser N., Fahlman G., Babul A.,Woods D., 1996, ApJ, 469, 73
Stompor R. *et al.* , 2001, ApJ, 561, L7
Sugiyama N, 1995, ApJS, 100, 281
Thomas P.A., Muanwong O., Kay S., Liddle A.R., 2002, MNRAS, 330, L48
Trümper J., 1993, Science, 260, 1769
Van Waerbeke, L, Mellier Y., Pello R., Pen U.-L., McCracken H.J., Jain B., 2002, A&A, submitted (astro-ph/0202503)
Viana P.T.P., Liddle A.R., 1996, MNRAS, 281, 323
Viana P.T.P., Liddle A.R., 1999, MNRAS, 303, 535
Viana P.T.P., Nichol R.C., Liddle A.R., 2002, ApJ, 569, L75
Voit G.M., Bryan G.L., Balogh M.L., Bower R.G., 2002, ApJ, in press (astro-ph/0205240)
White S.D.M., Frenk C.S., 1991, ApJ, 379, 52
White S.D.M., Navarro J.F., Evrard A.E., Frenk C.S., 1993, Nature, 366, 429